

# Absence of Local Fluctuating Dimers in Superconducting $\text{Ir}_{1-x}(\text{Pt,Rh})_x\text{Te}_2$

Runze Yu,<sup>1,†</sup> S. Banerjee,<sup>2</sup> H. C. Lei,<sup>1,††</sup> Ryan Sinclair,<sup>3</sup> M. Abeykoon,<sup>4</sup>

H. D. Zhou,<sup>3</sup> C. Petrovic,<sup>1</sup> Z. Guguchia,<sup>1,5</sup> and E. S. Bozin<sup>1,\*</sup>

<sup>1</sup>*Condensed Matter Physics and Materials Science Department,  
Brookhaven National Laboratory, Upton, NY 11973, USA\**

<sup>2</sup>*Department of Applied Physics and Applied Mathematics,  
Columbia University, New York, NY 10027, USA*

<sup>3</sup>*Department of Physics and Astronomy, University of Tennessee, Knoxville, Tennessee 37996, USA*

<sup>4</sup>*Photon Sciences Division, Brookhaven National Laboratory, Upton, NY 11973, USA and*

<sup>5</sup>*Department of Physics, Columbia University, New York, NY 10027, USA*

(Dated: June 12, 2018)

The compound  $\text{IrTe}_2$  is known to exhibit a transition to a modulated state featuring Ir-Ir dimers, with large associated atomic displacements. Partial substitution of Pt or Rh for Ir destabilizes the modulated structure and induces superconductivity. It has been proposed that quantum critical dimer fluctuations might be associated with the superconductivity. Here we test for such local dimer correlations and demonstrate their absence. X-ray pair distribution function approach reveals that the local structure of  $\text{Ir}_{0.95}\text{Pt}_{0.05}\text{Te}_2$  and  $\text{Ir}_{0.8}\text{Rh}_{0.2}\text{Te}_2$  dichalcogenide superconductors with compositions just past the dimer/superconductor boundary is explained well by a dimer-free model down to 10 K, ruling out the possibility of there being nanoscale dimer fluctuations in this regime. This is inconsistent with the proposed quantum-critical-point-like interplay of the dimer state and superconductivity, and precludes scenarios for dimer fluctuations mediated superconducting pairing.

Unconventional superconductivity (SC) often emerges in the proximity of symmetry breaking electronic and magnetic orders upon their destabilization by chemical modifications, external pressure and fields, as seen in a diverse variety of quantum systems [1–3]. The pairing mechanism remains elusive [4], in part because the role of fluctuations of adjacent ordered states and their ubiquity are not fully established and understood [5–7]. Studying such fluctuations is quite challenging [8], one of the reasons being the lack of the long range coherence [9]. When broken symmetry states, for example electronic states involving  $5d$  manifolds in  $\text{CuIr}_2\text{S}_4$  [10, 11] and  $\text{IrTe}_2$  [12, 13] where two  $\text{Ir}^{4+}$   $S=1/2$  bind into spinless spatially ordered dimers, are coupled to the lattice, footprints of their fluctuations become evident in the local atomic structure and can be studied indirectly using a local structural probe [14, 15] such as the atomic pair distribution function (PDF) analysis of powder diffraction data [16, 17]. Here we use x-ray PDF to probe the existence or absence of  $\text{Ir}^{4+}$ - $\text{Ir}^{4+}$  dimer fluctuations in doped  $\text{IrTe}_2$  superconductor, which yields information essential for bona fide considerations of dimer/SC entanglement in this system.

Trigonal metallic iridium ditelluride,  $\text{IrTe}_2$ , has garnered significant attention over the past several years following the discovery of bulk superconductivity ( $T_c \sim 3$  K) in its intercalated and substituted variants  $\text{IrTe}_2\text{:Pd}$  [18],  $\text{Ir}_{1-x}\text{Pt}_x\text{Te}_2$  [19],  $\text{Cu}_x\text{IrTe}_2$  [20], and  $\text{Ir}_{1-x}\text{Rh}_x\text{Te}_2$  [21]. Interestingly, the appearance of SC also follows the suppression of a long range ordered electronic state, in this case associated with charge disproportionation enabled  $\text{Ir}^{4+}$ - $\text{Ir}^{4+}$  dimerization [12, 13] established in  $\text{IrTe}_2$  at its symmetry lowering structural transition ( $T_s \sim 250$  K) [22]. This results in familiar domelike

phase diagrams, akin to those of high temperature SCs and recently discovered  $\text{Cu}_x\text{TiSe}_2$  [23],  $1\text{T-TaS}_2$  [24],  $1\text{T-TiSe}_2$  [25],  $\text{T}_d\text{-MoTe}_2$  [26],  $\text{ZrTe}_{3-x}\text{Se}_x$  [27], and  $2\text{H-TaSe}_{2-x}\text{S}_x$  [28] transition metal dichalcogenide superconductors, where destabilization of the charge density wave (CDW) order leads to SC. Importantly, in  $\text{Cu}_x\text{TiSe}_2$  quantum criticality associated with fluctuations of CDW order has been considered in relation to SC pairing [29, 30]. A perceived analogy with these systems prompted a hypothesis of quantum critical point (QCP) like interplay of SC and dimerization in  $\text{IrTe}_2$  derivatives [18], and speculations about dimer fluctuation mediated superconductivity [19, 31].

The importance of the  $\text{IrTe}_2$  lattice in facilitating the long range dimer order is well documented [32–34], with signatures of the dimer state found in a remarkable reduction of intradimer Ir-Ir (0.8 Å) and associated Te-Te (0.5 Å) distances [12], as illustrated in Fig. 1(a), (b). Despite this, and the importance of verifying the dimer fluctuations hypothesis, the utilization of experimental probes sensitive to presence/absence of local distortions has been surprisingly scarce. Existing reports based on extended x-ray absorption fine structure (EXAFS) spectroscopy focus on parent  $\text{IrTe}_2$  under ambient [35] and high pressure [36] conditions. The ambient study argues for persistence of *local* Ir dimers in the high temperature regime where the structure is undistorted trigonal on average [35]. Whilst this, if true, could hint at the presence of fluctuating dimers also in the superconducting compositions, experimental validation is still lacking.

Here we employ the PDF approach on superconducting compositions of two different  $\text{Ir}_{1-x}\text{A}_x\text{Te}_2$  families just across the dimer/SC boundary to explore for the first

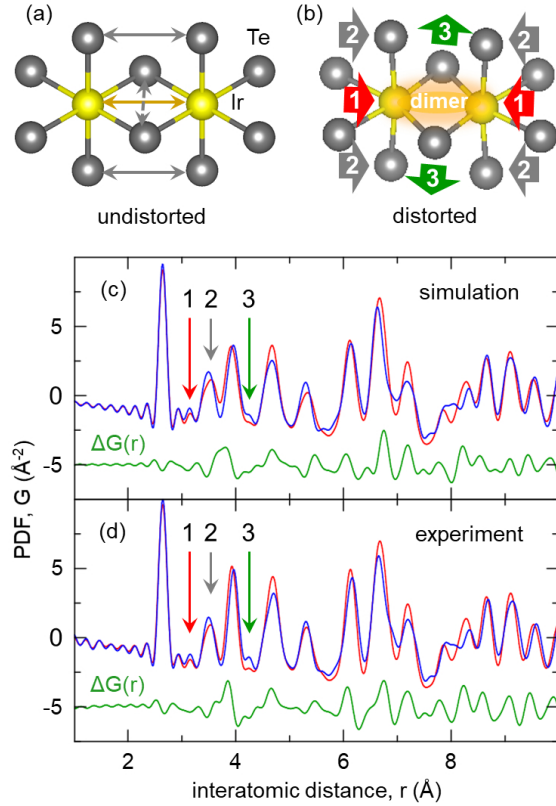


FIG. 1. (Color online) Sketch of the local atomic environments in  $\text{IrTe}_2$  for the (a) undistorted high temperature structure (trigonal  $\text{P}\bar{3}\text{m1}$ ), and (b) distorted low temperature structure (triclinic  $\text{P}\bar{1}$ ) featuring Ir-Ir and Te-Te dimers. Dimerization results in dramatic distortions of associated interatomic distances relative to the high temperature structure, as indicated by block arrows and described in the text. Comparison of PDFs (c) calculated from trigonal (red line) and triclinic (blue line) models, and (d) measured at 275 K (red line) and at 220 K (blue line). Enumerated vertical arrows in (c) and (d) mark features associated with these distortions.  $\Delta G(r)$  is the difference, offset for clarity.

time the existence of local dimer fluctuations. The PDF sensitivity to the presence of Ir-Ir dimers irrespective of the character of their ordering has been demonstrated in  $\text{CuIr}_2\text{S}_4$  [10, 37] and  $\text{Cu}(\text{Ir}_{1-x}\text{Cr}_x)_2\text{S}_4$  [38] spinels, where similar dimerization takes place on the Ir pyrochlore sublattice. When present, local dimers are clearly evident in the PDF of  $\text{IrTe}_2$  due to the large change in the Ir-Ir and Te-Te interatomic distances associated with them. Here we provide conclusive evidence that the dimers are absent in  $\text{Ir}_{0.95}\text{Pt}_{0.05}\text{Te}_2$  and  $\text{Ir}_{0.8}\text{Rh}_{0.2}\text{Te}_2$  down to 10 K. This unambiguously rules out the popular hypothesis of quantum dimer fluctuations in this regime and that such fluctuations play a role in SC pairing. Moreover, PDF finds no evidence for dimer fluctuations in  $\text{IrTe}_2$  at  $T > T_s$ , in stark contrast to previous EXAFS report [35].

Polycrystalline samples of  $\text{IrTe}_2$ ,  $\text{Ir}_{0.95}\text{Pt}_{0.05}\text{Te}_2$ , and  $\text{Ir}_{0.8}\text{Rh}_{0.2}\text{Te}_2$  were synthesized using standard solid-state

protocols, and were found to be single phase based on x-ray powder diffraction [39, 40]. Total scattering PDF experiments were performed at the 28-ID-2 beam line at the National Synchrotron Light Source II at Brookhaven National Laboratory, with 67.7 keV x-rays using the rapid acquisition mode with 60 s exposure/dataset [41]. The setup utilized *Perkin-Elmer* area detector and *Cryoindustries of America* cryostat for data collection between 10 K and 300 K on warming. The raw 2D diffraction data were integrated and converted to intensity versus  $Q$  using the software FIT2D [42], where  $Q$  is the magnitude of the scattering vector. Data reduction to measured total scattering structure functions,  $F(Q)$ , and their successive Sine Fourier transform up to a momentum transfer of  $Q_{\text{max}} = 25 \text{ \AA}^{-1}$  to obtain experimental PDFs,  $G(r)$ , were carried out using the PDFGETX3 [43] program. Models with  $\text{P}\bar{3}\text{m1}$  and  $\text{P}\bar{1}$  symmetry were used to describe nondimerized (Fig. 1(a)) and dimerized (Fig. 1(b)) structures, respectively, using the PDFGUI suite [44].

We begin by establishing qualitatively the sensitivity of our PDF data to the presence of dimers and concomitant structural distortions in  $\text{IrTe}_2$ . In the high temperature phase above  $T_s$  all Ir atoms are in identical  $\text{Te}_6$  octahedral environments displaying an edge-shared topology, Fig. 1(a), constituting trigonal symmetry average structure [45]. In the low temperature phase just below  $T_s$ , where the dimer patterns with a stripe morphology corresponding to  $\mathbf{q}_0 = 1/5(1, 0, 1)$  ordering are established [18, 32], Ir atoms subject to dimerization sit in distorted  $\text{Te}_6$  octahedral environments, Fig. 1(b), and the average symmetry lowers to triclinic [12]. Pairs of dimerization-affected  $\text{IrTe}_6$  octahedra exhibit dramatic structural rearrangements: Ir-Ir and Te-Te dimer distances reduce by 0.8  $\text{\AA}$  and 0.5  $\text{\AA}$  respectively, while the lateral Te-Te distance (common edge) elongates by 0.3  $\text{\AA}$  [12]. The distortions are depicted by enumerated block arrows in Fig. 1(b). Importantly, only  $\sim 6\%$  of all nearest neighbor Ir-Ir distances on triangular Ir planes of  $\text{IrTe}_2$  dimerize, in contrast to  $\text{CuIr}_2\text{S}_4$  where the fraction of dimerized Ir contacts is about 5 times larger [10].

We simulated PDF patterns for the average crystal structures for  $T > T_s$  (trigonal) and  $T < T_s$  (triclinic) using parameters from single crystal x-ray diffraction [12]. These are shown in Fig. 1(c) as red and blue profiles, respectively, with their difference plotted underneath. Changes in the interatomic distance distribution arising from dimerization as seen by PDF are marked by enumerated vertical arrows. Examination of the high and low temperature profiles reveals a redistribution of intensity in PDF peaks centered around 3.5  $\text{\AA}$  (Te-Te) and 3.9  $\text{\AA}$  (lattice repeat distance), whereas new peaks appear at around 3.1  $\text{\AA}$  (Ir-Ir dimer), 3.4  $\text{\AA}$  (Te-Te dimer), and 4.2  $\text{\AA}$  (common Te-Te edge). It is evident that the Ir-Ir dimer signal at 3.1  $\text{\AA}$  is rather weak, as compared to that observed in  $\text{CuIr}_2\text{S}_4$  spinel [37], and is barely visible above the parapet of termination ripples caused by

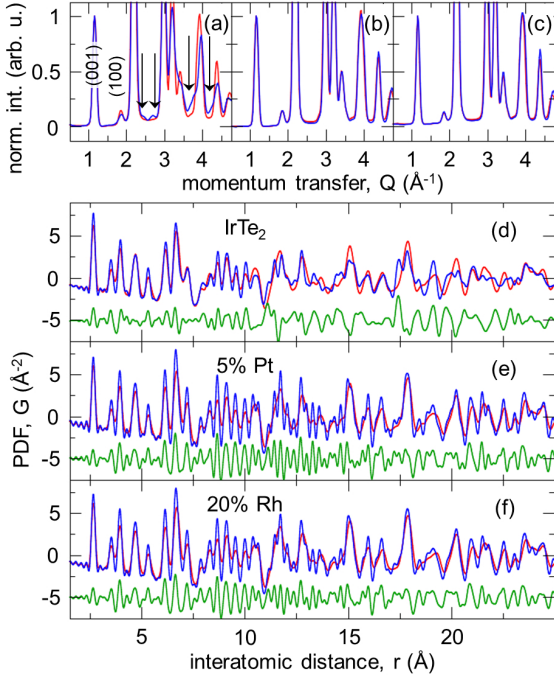


FIG. 2. (Color online) Azimuthally integrated 2D diffraction patterns of  $\text{Ir}_{1-x}(\text{Pt,Rh})_x\text{Te}_2$  for 300 K (red line) and 10 K (blue line) over a narrow range of momentum transfer,  $Q$ , for (a)  $x=0$ , (b)  $x=0.05$  Pt, and (c)  $x=0.2$  Rh. All patterns are normalized by the intensity of (001) reflection ( $P\bar{3}m1$  indexing). Vertical arrows in (a) indicate superlattice reflections observed in 10 K data. Corresponding PDFs are compared in (d), (e), and (f), respectively, with differences shown underneath and offset for clarity.

the finite range of the Fourier transform. This comes about due to different dimer densities in the two materials. However, this analysis shows that, despite this relatively weaker signal, the PDF is still sensitive to the presence or absence of local dimers.

Experimental PDFs of  $\text{IrTe}_2$  for temperatures straddling  $T_s$  are compared in Fig. 1(d), where the 275 K (red profile,  $T > T_s$ ) and the 220 K (blue profile,  $T < T_s$ ) data and their difference are displayed. A qualitative assessment readily demonstrates that all dimerization features described above and highlighted in the calculated PDFs, which contain the impact of the dimers, are well reproduced in the experimental PDF data. This clearly establishes the PDF sensitivity to dimer structural signatures and their detectability in our data. Comparisons in Figs. 1 (c) and (d) also indicate that the dimers *disappear* in the local structure above  $T_s$ , as is further confirmed by explicit modeling that we discuss later. Notably, proposed order-disorder scenario for the dimerization transition [35] is at odds with this observation. The first-order nature of the transition [22, 32] also argues against the persistence of local fluctuating dimers above  $T_s$ .

Samples with SC compositions display qualitatively different behavior on all lengthscales accessible by our

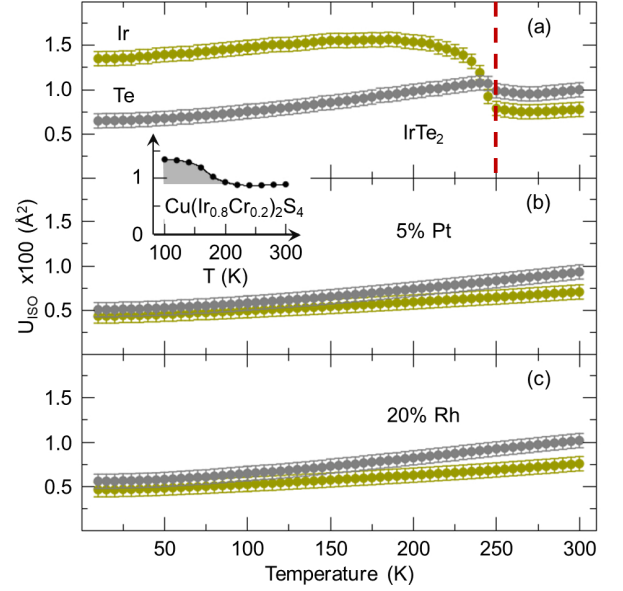


FIG. 3. (Color online) Temperature dependence of the isotropic ADPs of Ir (olive symbols) and Te (gray symbols) in  $\text{Ir}_{1-x}(\text{Pt,Rh})_x\text{Te}_2$  obtained from  $P\bar{3}m1$  model fits to (a)  $x=0$ , (b)  $x=0.05$  Pt, and (c)  $x=0.2$  Rh sample data over the 10 K–300 K temperature range. Inset: detection of onset of dimer fluctuations from temperature dependent Ir-ADP in 20% Cr-doped  $\text{CuIr}_2\text{S}_4$ , where Ir-Ir dimerization sets in below 200 K on a nanometer length-scale *only*, while the long range dimer order is absent at all temperatures [38]. Such behavior is *not* observed in (b) and (c) for superconducting  $\text{Ir}_{1-x}(\text{Pt,Rh})_x\text{Te}_2$ .

measurements. When the average  $\text{IrTe}_2$  symmetry is lowered and the long range dimer order is established, superlattice reflections appear in the integrated diffraction patterns, as seen in Fig. 2(a) where 10 K and 300 K are compared. In contrast, no such features are observed in  $\text{Ir}_{0.95}\text{Pt}_{0.05}\text{Te}_2$  (Fig. 2(b)) and  $\text{Ir}_{0.8}\text{Rh}_{0.2}\text{Te}_2$  (Fig. 2(c)) data at any temperature, consistent with the average symmetry remaining trigonal down to 10 K and no long range dimer order, as expected from the monotonic temperature variation of susceptibility and electrical resistivity [19, 21]. Importantly, the dimers are also not observed at low temperature on intermediate and short lengthscales probed by the PDF. When symmetry lowering occurs, this causes redistribution of PDF intensities and overall broadening of the PDF patterns due to the appearance of new interatomic distances. Conversely, temperature lowering sharpens the PDF features as a consequence of decreasing the amplitudes of thermal vibrations [17]. Both effects are present in  $\text{IrTe}_2$  PDFs, Fig. 2(d), where the 300 K profile is observably sharper than that of 10 K at intermediate  $r$ , and their difference reveals a change corresponding to a superposition of these two opposite effects. Figs. 2 (e) and (f) show 300 K and 10 K data for superconducting samples. Whilst there are also dramatic changes evidenced in the respective differ-

ence curves, this is qualitatively different from what is seen in  $\text{IrTe}_2$ .

It can be shown through a semiempirical scaling procedure that high and low temperature PDFs of doped samples can be successfully morphed into each other, whereas such a procedure fails in the case of  $\text{IrTe}_2$ . This arguably indicates that the changes in the SC samples are likely caused solely by thermal effects, without symmetry lowering, whereas the actual symmetry breaking is needed to explain the changes in the parent system (see Supplemental Material for details). To further corroborate this, an undistorted trigonal model was refined in the  $r$ -space against the PDF data in 10 K–300 K range for all samples, and the obtained atomic displacement parameters (ADPs) monitored, Fig. 3. While in  $\text{IrTe}_2$  both ADPs of Ir and Te initially drop linearly with temperature, Fig. 3(a), they exhibit an abrupt jump at the onset of the dimerization transition, denoted by vertical dashed red line in the figure. This nominally implies “disorder”, but actually reflects the inadequacy of the trigonal model to explain the symmetry breaking and underlying dimerization encoded in the data. In contrast, no such jumps are observed for  $\text{Ir}_{0.95}\text{Pt}_{0.05}\text{Te}_2$  (Fig. 3(b)) and  $\text{Ir}_{0.8}\text{Rh}_{0.2}\text{Te}_2$  (Fig. 3(c)) in the entire temperature range studied. It is important to realize that jumps in ADPs are not only observed across long range symmetry breaking transitions, but also in cases when there is only a local structure change in the absence of any macroscopic transitions. The inset in Fig. 3 exemplifies such a situation seen in 20% Cr-doped  $\text{CuIr}_2\text{S}_4$ , where *local* Ir-Ir dimerization sets in just below 200 K, in the absence of long range dimer order at any temperature in that system [38]. This demonstrates that there is neither average nor local symmetry lowering in  $\text{Ir}_{0.95}\text{Pt}_{0.05}\text{Te}_2$  and  $\text{Ir}_{0.8}\text{Rh}_{0.2}\text{Te}_2$  down to 10 K.

Finally, we consider the actual fits of the trigonal structure model to various PDF data over the 10 Å range, shown in Fig. 4 as solid red lines and open blue symbols, respectively. This undistorted dimer-free model explains the  $\text{IrTe}_2$  300 K data exceptionally well, Fig. 4(a), as evident from the flat difference curve and a low fit residual value of  $r_w \sim 4\%$ . The same model fails to explain the  $\text{IrTe}_2$  data at 10 K ( $r_w \sim 15\%$ ), in Fig. 4(b), as expected, given that at that temperature long range dimer order is well established and that the attempted dimer-free model is strictly inadequate. Importantly, this failed fit charts substantial misfits in the difference curve that would reveal the presence of dimers in the data when they are confronted with a dimer-free model. Figs. 4(c) and (d) show the results of such a fitting attempt carried out on 10 K  $\text{Ir}_{0.95}\text{Pt}_{0.05}\text{Te}_2$  and  $\text{Ir}_{0.8}\text{Rh}_{0.2}\text{Te}_2$  data, respectively. Not only do the corresponding difference curves not display the features observed in Fig. 4(b), but the fits of the trigonal model in fact agree rather well with the data ( $r_w \sim 5\%$ ). The local structure at 10 K for these compositions can be well explained by a dimer-free model. This

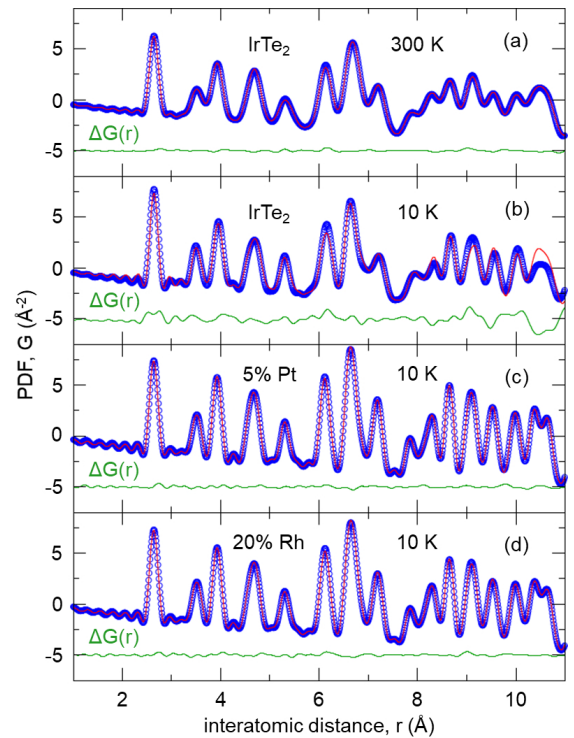


FIG. 4. (Color online) Fits of trigonal structure model (solid red lines) to experimental PDF data (open blue symbols) of  $\text{IrTe}_2$  sample at (a) 300 K and (b) 10 K, 5 % Pt substituted sample at 10 K (c), and 20 % Rh substituted sample at 10 K (d). The difference between the data and the model,  $\Delta G(r)$ , plotted below, is offset for clarity. See text for details.

quantitative analysis validates the aforementioned qualitative conclusions about the absence of dimer fluctuations in the high temperature phase of the parent system as well as at 10 K in superconducting compositions just past the dimer/SC boundary. The transition in  $\text{IrTe}_2$  is argued to originate from a uniform lattice deformation combined with charge ordering and subsequent Ir dimerization [33]. According to a recent high pressure study of  $\text{Ir}_{1-x}\text{Pt}_x\text{Te}_2$ , the structural transition triggers charge ordering and dimerization [34]. This implies that fluctuations associated with the putative QCP are expected to appear not only in the electronic, but also in the structural channel. However, the PDF results presented here do not show any evidence that would support this picture.

In conclusion, by using state of the art x-ray total scattering based PDF approach we establish the first direct evidence for the absence of local dimer fluctuations in the phase diagrams of  $\text{Ir}_{1-x}\text{Pt}_x\text{Te}_2$  and  $\text{Ir}_{1-x}\text{Rh}_x\text{Te}_2$  beyond the dimer/superconductor phase boundary. The dimer fluctuations are also absent in the parent  $\text{IrTe}_2$  in the temperature regime above the structural phase transition. These results imply that dimer fluctuations are not a relevant part of the phase diagram of  $\text{IrTe}_2$  based systems and thus their role in the superconducting pair-



ing is implausible. The results provide important new constraints for theoretical considerations of the complex interplay between superconductivity and other electronic orders in this class of materials.

Work at Brookhaven National Laboratory was supported by US DOE, Office of Science, Office of Basic Energy Sciences (DOE-BES) under contract de-sc00112704. R. Sinclair and H. D. Zhou acknowledge support from NSF-DMR-1350002. We are grateful to John Tranquada, Simon Billinge, Ian Robinson, and Alexei Tsvelik for fruitful discussions and critical comments.

---

\* bozin@bnl.gov

<sup>†</sup>Present address: Institute of Physics, Chinese Academy of Science, Beijing, 100190, Peoples Republic of China

<sup>††</sup> Present address: Department of Physics, Renmin University, Beijing 100872, Peoples Republic of China

- [1] D. N. Basov and A. V. Chubukov, *Nature Phys.* **7**, 272 (2011).
- [2] G. Saito and Y. Yoshida, *Chem. Rec.* **11**, 124 (2011).
- [3] L. Jiao, Y. Chen, Y. Kohama, D. Graf, E. Bauer, J. Singleton, J. Zhu, Z. Weng, G. Pang, T. Shang, et al., *Proc. Natl. Acad. Sci. USA* **112**, 673 (2015).
- [4] M. R. Norman, *Science* **332**, 196 (2011).
- [5] P. A. Lee, N. Nagaosa, and X. Wen, *Rev. Mod. Phys.* **78**, 17 (2006).
- [6] J. Chang, E. Blackburn, A. T. Holmes, N. B. Christensen, J. Larsen, J. Mesot, R. Liang, D. A. Bonn, W. N. Hardy, A. Watenphul, et al., *Nature Phys.* **8**, 871 (2010).
- [7] R. Comin, A. Frano, M. Yee, Y. Yoshida, H. Eisaki, E. Schierle, E. Weschke, R. Sutarto, F. He, A. Soumyanarayanan, et al., *Science* **343**, 390 (2014).
- [8] S. A. Kivelson, I. P. Bindloss, E. Fradkin, V. Oganessian, J. M. Tranquada, A. Kapitulnik, and C. Howald, *Rev. Mod. Phys.* **75**, 1201 (2003).
- [9] S. J. L. Billinge and I. Levin, *Science* **316**, 561 (2007).
- [10] P. G. Radaelli, Y. Horibe, M. J. Gutmann, H. Ishibashi, C. H. Chen, R. M. Ibberson, Y. Koyama, Y. S. Hor, V. Kiryukhin, and S. W. Cheong, *Nature* **416**, 155 (2002).
- [11] D. I. Khomskii and T. Mizokawa, *Phys. Rev. Lett.* **94**, 156402 (2005).
- [12] G. L. Pascut, K. Haule, M. J. Gutmann, S. A. Barnett, A. Bombardi, S. Artyukhin, T. Birol, D. Vanderbilt, J. J. Yang, S. Cheong, et al., *Phys. Rev. Lett.* **112**, 086402 (2014).
- [13] T. Toriyama, M. Kobori, T. Konishi, Y. Ohta, K. Sugimoto, J. Kim, A. Fujiwara, S. Pyon, K. Kudo, and M. Nohara, *J. Phys. Soc. Jpn* **83**, 033701 (2014).
- [14] J. Lee, K. Fujita, K. McElroy, J. A. Slezak, M. Wang, Y. Aiura, H. Bando, M. Ishikado, T. Masui, J. Zhu, et al., *Nature* **442**, 546 (2006).
- [15] E. S. Božin, M. Schmidt, A. J. DeConinck, G. Paglia, J. F. Mitchell, T. Chatterji, P. G. Radaelli, T. Proffen, and S. J. L. Billinge, *Phys. Rev. Lett.* **98**, 137203 (2007).
- [16] S. J. L. Billinge, *J. Solid State Chem.* **181**, 1695 (2008).
- [17] T. Egami and S. J. L. Billinge, *Underneath the Bragg peaks: structural analysis of complex materials* (Elsevier, Amsterdam, 2012), 2nd ed.
- [18] J. J. Yang, Y. J. Choi, Y. S. Oh, A. Hogan, Y. Horibe, K. Kim, B. I. Min, and S. Cheong, *Phys. Rev. Lett.* **108**, 116402 (2012).
- [19] S. Pyon, K. Kudo, and M. Nohara, *J. Phys. Soc. Jpn* **81**, 053701 (2012).
- [20] M. Kamitani, M. S. Bahramy, R. Arita, S. Seki, T. Arima, Y. Tokura, and S. Ishiwata, *Phys. Rev. B* **87**, 180501 (2013).
- [21] K. Kudo, M. Kobayashi, S. Pyon, and M. Nohara, *J. Phys. Soc. Jpn* **82**, 085001 (2013).
- [22] N. Matsumoto, K. Taniguchi, R. Endoh, H. Takano, and S. Nagata, *J. Low Temp. Phys.* **117**, 1129 (1999).
- [23] E. Morosan, H. W. Zandbergen, B. S. Dennis, J. W. G. Bos, Y. Onose, T. Klimczuk, A. P. Ramirez, N. P. Ong, and R. J. Cava, *Nature Phys.* **2**, 544 (2006).
- [24] B. Sipos, A. F. Kusmartseva, A. Akrap, H. Berger, L. Forro, and E. Tutis, *Nature Mater.* **7**, 960 (2008).
- [25] A. F. Kusmartseva, B. Sipos, H. Berger, L. Forro, and E. Tutis, *Phys. Rev. Lett.* **103**, 236401 (2009).
- [26] Z. Guguchia, F. von Rohr, Z. Shermadini, A. T. Lee, S. Banerjee, A. R. Wieteska, C. A. Marianetti, B. A. Frandsen, H. Luetkens, Z. Gong, et al., *Nat. Commun.* **8**, 1082 (2017).
- [27] X. Zhu, W. Ning, L. Li, L. Ling, R. Zhang, J. Zhang, K. Wang, Y. Liu, L. Pi, Y. Ma, et al., *Sci. Rep.* **6**, 26974 (2016).
- [28] L. Li, X. Deng, Z. Wang, Y. Liu, M. Abeykoon, E. Dooryhee, A. Tomic, Y. Huang, J. B. Warren, E. S. Bozin, et al., *npj Quantum Materials* **2**, 11 (2017).
- [29] H. Barath, M. Kim, J. F. Karpus, S. L. Cooper, P. Abbamonte, E. Fradkin, E. Morosan, and R. J. Cava, *Phys. Rev. Lett.* **100**, 106402 (2008).
- [30] A. H. Castro Neto, *Phys. Rev. Lett.* **86**, 4382 (2001).
- [31] J. Dai, K. Haule, J. J. Yang, Y. S. Oh, S. Cheong, and W. Wu, *Phys. Rev. B* **90**, 235121 (2014).
- [32] Y. S. Oh, J. J. Yang, Y. Horibe, and S. Cheong, *Phys. Rev. Lett.* **110**, 127209 (2013).
- [33] K. Kim, S. Kim, K. Ko, H. Lee, J. Park, J. J. Yang, S. Cheong, and B. I. Min, *Phys. Rev. Lett.* **114**, 136401 (2015).
- [34] O. Ivashko, L. Yang, D. Destraz, E. Martino, Y. Chen, C. Y. Guo, H. Q. Yuan, A. Pisoni, P. Matus, S. Pyon, et al., *Sci. Rep.* **7**, 17157 (2017).
- [35] B. Joseph, M. Bendele, L. Simonelli, L. Maugeri, S. Pyon, K. Kudo, M. Nohara, T. Mizokawa, and N. L. Saini, *Phys. Rev. B* **88**, 224109 (2013).
- [36] E. Paris, B. Joseph, A. Iadecola, C. Marini, H. Ishii, K. Kudo, S. Pascarelli, M. Nohara, T. Mizokawa, and N. L. Saini, *Phys. Rev. B* **93**, 134109 (2016).
- [37] E. S. Božin, A. S. Masadeh, Y. S. Hor, J. F. Mitchell, and S. J. L. Billinge, *Phys. Rev. Lett.* **106**, 045501 (2011).
- [38] E. S. Božin, K. R. Knox, P. Juhás, Y. S. Hor, J. F. Mitchell, and S. J. L. Billinge, *Sci. Rep.* **4**, 4081 (2014).
- [39] H. Cao, B. C. Chakoumakos, X. Chen, J. Yan, M. A. McGuire, H. Yang, R. Custelcean, H. D. Zhou, D. J. Singh, and D. Mandrus, *Phys. Rev. B* **88**, 115122 (2013).
- [40] N. Lazarevic, E. S. Bozin, M. Scepovic, M. Opacic, H. Lei, C. Petrovic, and Z. V. Popovic, *Phys. Rev. B* **89**, 224301 (2014).
- [41] P. J. Chupas, X. Qiu, J. C. Hanson, P. L. Lee, C. P. Grey, and S. J. L. Billinge, *J. Appl. Crystallogr.* **36**, 1342 (2003).
- [42] A. P. Hammersley, S. O. Svenson, M. Hanfland, and D. Hauserman, *High Pressure Res.* **14**, 235 (1996).

- [43] P. Juhás, T. Davis, C. L. Farrow, and S. J. L. Billinge, J. Appl. Crystallogr. **46**, 560 (2013).
- [44] C. L. Farrow, P. Juhás, J. Liu, D. Bryndin, E. S. Božin, J. Bloch, T. Proffen, and S. J. L. Billinge, J. Phys: Condens. Mat. **19**, 335219 (2007).
- [45] E. F. Hockings and J. G. White, J. Phys. Chem. **64**, 1042 (1960).